PERGAMON

International Journal of Solids and Structures 37 (2000) 7617–7631

INTERNATIONAL JOURNAL OF SOLIDS and STRUCTURES

www.elsevier.com/locate/ijsolstr

Three-dimensional elastic stress fields near notches in finite thickness plates

Zhenhuan Li [a], Wanlin Guo [a,*], Zhenbang Kuang [b]

[a] *The National Key Laboratory of Mechanical Structural Strength and Vibration, Xi'an Jiaotong University, Xi'an 710049, People's Republic of China*

[b] *Department of Engineering Mechanics, Shanghai Jiaotong University, Shanghai 200240, People's Republic of China*

Received 15 July 1999

Abstract

Based on detailed three-dimensional finite element (3D FE) analyses, elastic notch-root fields in plates with different thicknesses and notch configurations subjected to uniaxial tension have been investigated. By comparing with the planar notch-root fields and crack-tip fields, the following characteristics of the 3D stress–strain fields near the notch front are revealed: (1) The plate thickness and notch configuration have obvious effects on the stress concentration factor (SCF) K_t, which is higher in finite thickness plates than in plane stress and plane strain cases. (2) The variation of the opening stress normalized by its value at the notch root with a distance x from the root normalized by the root radius ρ is insensitive to the notch configuration and the plate thickness and coincides well with the two-dimensional (2D) planar solution when $x/\rho < 0.75$. (3) Strong 3D effects exist within a radius of about three-eighth the plate thickness from the notch root. Further away from the root, the through-thickness variation of field quantities decreases and, at the radial distance of approximately 1.25 times the plate thickness, all of the through-thickness changes disappear completely. At least for notches with opening angles less than 90°, these "2D–3D" transition distances and the variations of the out-of-plane constraint normalized by its value at the notch root with a distance x from the root normalized by the plate thickness B are essentially independent of the notch configuration and plate thickness. (4) In the 3D-effect zone, the gradient of the out-of-plane strain ε_{zz} in the thickness direction is significant near the free surface in thick plates. On the free surface, ε_{zz} can be 3.5 times as high as the value on the mid-plane. It is also found that the in-plane stress ratio in an arbitrary thickness plate coincides very well with the 2D solutions within a distance of about three-tenth of the root radius from the notch root.

Keywords: Finite thickness plate; Notch configuration; Three-dimensional effect; Linear elastic; Finite element

1. Introduction

Knowledge of stress–strain concentrations in the neighborhood of stress raisers, such as notches and holes is frequently required for an accurate design of structural components. Particularly, in modern

* Corresponding author. Tel.: +86-29-326-8751; fax: +86-29-323-7910.
E-mail address: guowl@xjtu.edu.cn (W. Guo).

0020-7683/00/$ - see front matter
PII: S0020-7683(99)00311-X

structures designed to carry high loads, stress concentration becomes the most serious issue in the safe design and maintenance of machines and structures has long been a concern.

Since the classical complex variable solutions by Muskhelishvili (1963) and Savin (1961) for holes in infinite bodies, many efforts have been made to achieve rational solutions for holes and notches in infinite plates and empirical formulae for more practical cases (Creager and Paris, 1967; Kuang, 1982; Sadowsky and Sternberg, 1947; Shin et al., 1994; Kujawski, 1991). However, most of this kind of work is limited to two-dimensional (2D) problems.

It is well known that, due to the localized perturbation of stress fields, there exists a strong three-dimensional (3D) region in the neighborhood of the notch root. In such a situation, four additional scales: the notch depth, the notch opening angle, the notch-root radius and the thickness of the plate have to be introduced. This substantially increases the difficulty to obtain rational solutions for the local stress fields in the vicinity of the notch root. Fifty years ago, by the use of series expansion and taking finite terms into account, Sternberg et al. (1949) obtained an excellent approximate solution for 3D stress distributions in the neighborhood of a circular hole in an infinite plate of arbitrary thickness. Detailed analyses for the out-of-plane stress constraint were provided, but for stress concentrations only a brief discussion was given. By a similar method, Sadowsky and Sternberg (1949) obtained the stress distribution near a general triaxial ellipsoidal cavity in an infinite elastic body subjected to a triaxial tension. Based on careful examinations of the solutions of Sadowsky and Sternberg (1947, 1949), Xu et al. (1996) proposed an empirical modification to the 2D-notch solutions (Xu et al., 1995) to take the 3D effects into account. Recently, both the Cosserat's and Kane–Mindlin's plate theories (Kane and Mindlin, 1956 were used by Krishnaswamy et al. (1998) together with a stress function method to investigate the stress concentration around a circular hole in a finite thickness plate. Although they obtained the correct stress concentration factor (SCF) 3, in infinite thin plates, the SCF in their solution decreases remarkably when the plate becomes thicker and approaches 2 as the thickness becomes infinitely large, which is far from the plane strain value 3. However, for a wide variety of 3D-notch configurations, to our knowledge, even a numerical study is hard to find in the literature. It is also suspectable whether the existing plate theories can predict the effects of thickness on the field quantities for different 3D-notch configurations.

In this article, in order to reveal the natural characteristics of the 3D-notch fields, detailed FE analyses are conducted for different notch configurations and thickness of plates. By comparing with the plane-stress and plane-strain solutions, various aspects of the 3D fields near the notch root are investigated carefully.

2. Computational procedures

2.1. Definitions

The problems considered here are double-edge U-notches with different depths, a V-notch and a circular hole in finite thickness plates subjected to a uniaxial tension, as shown in Fig. 1. The notch depth is a, the notch-root radius is ρ, the width of the plate is $2W$, and the thickness and height of the plate are B and $2H$, respectively. The opening angle of the V-notch is 2β.

The geometrical parameters of the notched specimens analyzed are:

1. Double edge semi-circular notch (denoted by SC): $H = 10$ mm, $\rho = 0.1$ mm, $a/\rho = 1.0$, $a/W = 0.025$.
2. Double edge U-notch (denoted by UN): $H = 10$ mm, $\rho = 0.1$ mm, $a/\rho = 5.5$, $a/W = 0.133$; $a/\rho = 11$, $a/W = 0.22$; $a/\rho = 21$, $a/W = 0.35$, respectively.
3. Double edge V-notch (denoted by VN): $H = 10$ mm, $\rho = 0.4$ mm, $a/\rho = 10.0$, $a/W = 0.40$, $\beta = 45^\circ$.
4. Circular hole (denoted by Hole): $H = 10$ mm, $\rho = 0.1$ mm, $a/W = 0.025$, $a/\rho = 1.0$.

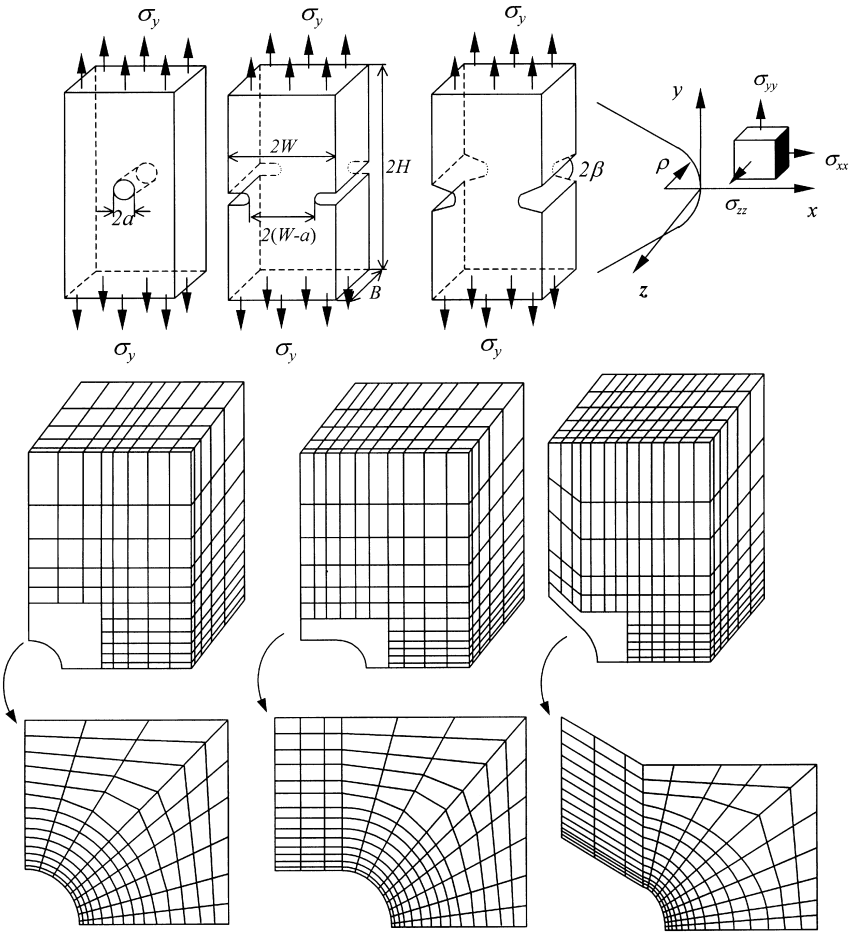

Fig. 1. Illustration of the problem and the 3D finite element model.

For convenience, the rectangular coordinates (x, y, z) is adopted in this article. The origin of the coordinate system is at the notch root and the plate is between $z = \pm B/2$. To describe the 3D characteristics of the notch stress fields more clearly, two constraint parameters are introduced:

(1) *Out-of-plane stress constraint factor*

$$T_z = \frac{\sigma_{zz}}{\sigma_{xx} + \sigma_{yy}}, \tag{1}$$

$T_z = 0$ for the plane stress state and $T_z = v$ for the plane strain state. For the finite thickness plate, $0 \leqslant T_z \leqslant v$, where v is the Poisson ratio of the material.

(2) *In-plane stress ratio*

$$T_x = \frac{\sigma_{xx}}{\sigma_{yy}}. \tag{2}$$

The definition of the SCF is

$$K_t = \frac{\sigma_{yy0}}{\sigma_{\text{net}}} \quad \text{at } x = y = 0, \tag{3}$$

where $\sigma_{net} = \sigma_y W/(W-a)$ is the mean stress of the net section on the ligament. σ_y is the applied stress at the ends of the plate. σ_{yy0} is the opening stress at the notch root. In the present analysis, K_t takes at the first Gauss point ahead of the notch root, or

$$K_t = \frac{\sigma_{yy0}}{\sigma_{net}} \quad \text{at } x/\rho = 0.011.$$

2.2. Finite element model

Only one-eighth of each specimen (region $y \geqslant 0$, $0 \leqslant z \leqslant B/2$ and half-width) is modeled with finite elements, as the problem has reflective symmetry with respect to the mid-plane ($z/B = 0$) and the plane ($x = (W-a)/2$), and the ligament plane ($y = 0$). The FE mesh is constructed with 20-node hexahedron isoparametric elements as shown in Fig. 1. Five planar layers are divided through the half-thickness of the plate. To accommodate the variations of the field quantities through the plate, the thickness of each successive element layer is gradually reduced toward the free surface ($z = B/2$). Within each layer, 14 focused rings of elements enclose the notch root. The size of each ring increases gradually with radial distance from the notch root. These 3D models represent a compromise between the required level of mesh refinement to solve the in-plane and through-thickness gradients of the stress fields and the extensive computation times required for each analysis.

In our 3D FE computations, Poisson's ratio $v = 0.333$ and Young's modulus $E = 200$ GPa are chosen.

3. Analyses of the computational results

3D FE results for $B/\rho = 0.01$–40 and the corresponding plane stress and plane strain solutions are obtained using the FE code ANSYS-5.4. The thickness effect on the stress concentrations is analyzed in Section 3.1. Following that the out-of-plane and in-plane constraints near the notch root are studied in Sections 3.2 and 3.3. Finally, the description of the stress fields in the 3D-perturbation region is provided.

3.1. The stress concentration factor

Similar to the stress intensity factor in the crack problem, the SCF K_t is an important parameter scaling the extent of stress raisers around notches. For different notch configurations, the variations of SCF $(K_t)_{m-p}$ on the mid-plane ($2z/B = 0$) against the dimensionless plate thickness (B/ρ) are plotted in Fig. 2, where $(K_t)_{m-p}$ is normalized by the plane stress value $(K_t)_{p-\sigma}$ of the corresponding notch configuration. It is interesting to find that $(K_t)_{m-p}$ in a finite thickness plate is not a monotonic function of thickness. $(K_t)_{m-p}$ increases from its plane stress value $(K_t)_{p-\sigma}$ at $B/\rho = 0$ to its peak value $K_{t\max}$ at about $B/\rho \approx 3$–8, then decreases gradually with increasing B/ρ and tends to its plane strain value when B/ρ becomes large enough. It is important to observe that the curves $(K_t)_{m-p}/(K_t)_{p-\sigma}$–$B/\rho$ are nearly independent of the notch configuration before $(K_t)_{m-p}/(K_t)_{p-\sigma}$ reaches its peak value. After the peak value, $(K_t)_{m-p}/(K_t)_{p-\sigma}$ becomes a decreasing function of B/ρ, and the decreasing rate is higher for the shallower notch.

Fig. 3(a) shows the through-thickness variations of K_t in the plates of different notch configurations for $B/\rho = 2$. In Fig. 3, the SCF K_t is normalized by $(K_t)_{m-p}$. The through-thickness variations of $K_t/(K_t)_{m-p}$ are insensitive to the notch geometry except near the free surface, where $K_t/(K_t)_{m-p}$ is lower for a deeper notch. For different notch configurations, the average value of $K_t/(K_t)_{m-p}$ through the thickness is nearly the same, about 0.92. $(K_t)_{m-p}$ at the mid-plane is 25% higher than K_t at the free surface for $B/\rho = 2$.

Thickness effects on the through-thickness variations of K_t are shown in Fig. 3(b) for U-notches. In the middle region, the variation of K_t with $2z/B$ is weak, and the greater the dimensionless thickness (B/ρ), the

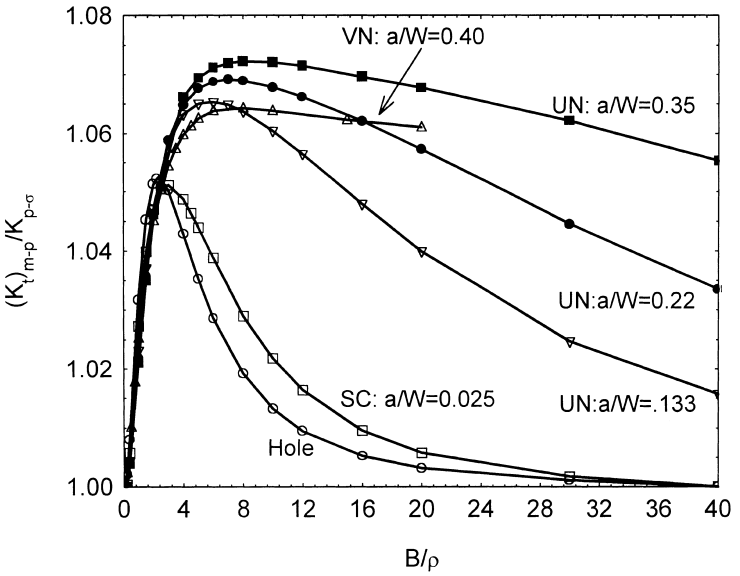

Fig. 2. The variations of the stress concentration factor on the mid-plane with a dimensionless thickness for different notch configurations.

more stable the K_t becomes in this region. In contrast, the K_t at the free surface becomes lower as B/ρ increases. It is also shown that, K_t in the middle region in a finite thickness plate is higher than that in the plane stress and plane strain states. Near the free surface, however, K_t decreases rapidly and becomes lower than the corresponding plane stress and plane strain values. For a notch configuration with large B/ρ, the K_t at the free surface is too low to reflect the overall stress concentration.

Figs. 2 and 3 also show that it is risky to use K_t measured at the free surface or calculated by 2D theories in the engineering design.

From the above discussion, it can be found that the normalized SCF $K_t/(K_t)_{m-p}$ can be approximately expressed as a function of B/ρ and z/B by

$$\frac{K_t}{(K_t)_{m-p}} = f(B/\rho, z/B). \tag{4}$$

3.2. Three-dimensionality near the notch front

As is well known, for a sufficiently thin cracked plate, a strong 3D field is observed within the radius of half the plate thickness from the tip and a "2D–3D" transition state persists up to a radial distance from the crack front of 1.5 times the thickness (Nakamura and Parks, 1988, 1990). In Fig. 4(a) and (b), the distributions of the out-of-plane stress constraint $(T_z)_{m-p}$ on the mid-plane $2z/B = 0$ in front of notches are presented for different notch depths a/W with $B/\rho = 2$ and different dimensionless thicknesses B/ρ with $a/W = 0.133$, respectively. In the figures, $(T_z)_{m-p}$ is normalized by $(T_{z0})_{m-p}$, the out-of-plane constraint at the notch root and, the distance (x) from the notch root is normalized by the thickness (B). Fig. 4 shows that a positive $(T_z)_{m-p}$ exists within about $x/B < 0.375$. As x/B increases, $(T_z)_{m-p}$ dips slightly below zero between $0.375 < x/B < 1.25$, and for larger x/B, $(T_z)_{m-p}$ disappears and the plane stress becomes the dominant state. It is surprising that within the 3D-perturbation region the curves $(T_z)_{m-p}/(T_{z0})_{m-p} \sim x/B$ are nearly independent of both the notch configuration and B/ρ. Therefore, referring to the form of the

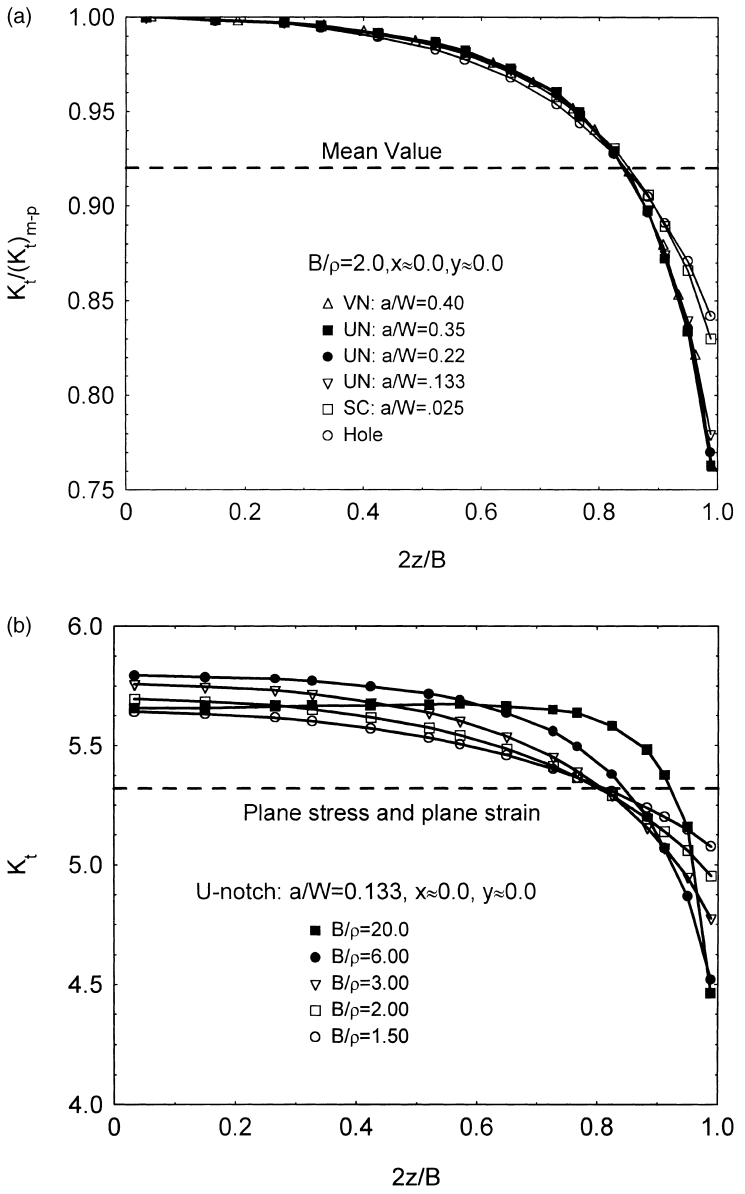

Fig. 3. The through-thickness variations of the stress concentration factor in plates with (a) different notch configurations and, (b) different dimensionless thicknesses.

solution for an infinite plate having a circular hole (Timoshenko and Goodier, 1970), we can approximate the distribution of $(T_z)_{m-p}$ within the 3D-effect zone in the vicinity of notches by

$$\frac{(T_z)_{m-p}}{(T_{z0})_{m-p}} = 1 - c\left(1 + \alpha\frac{x}{B}\right)^{-2} + c\left(1 + \alpha\frac{x}{B}\right)^{-4}. \tag{5}$$

By fitting the 3D FE results of the notches with different configurations, it can be obtained that $c = 4.35$, and $\alpha = 0.628$ with a maximum deviation of 0.0554 (see Fig. 4(a)). In order to validate approximate

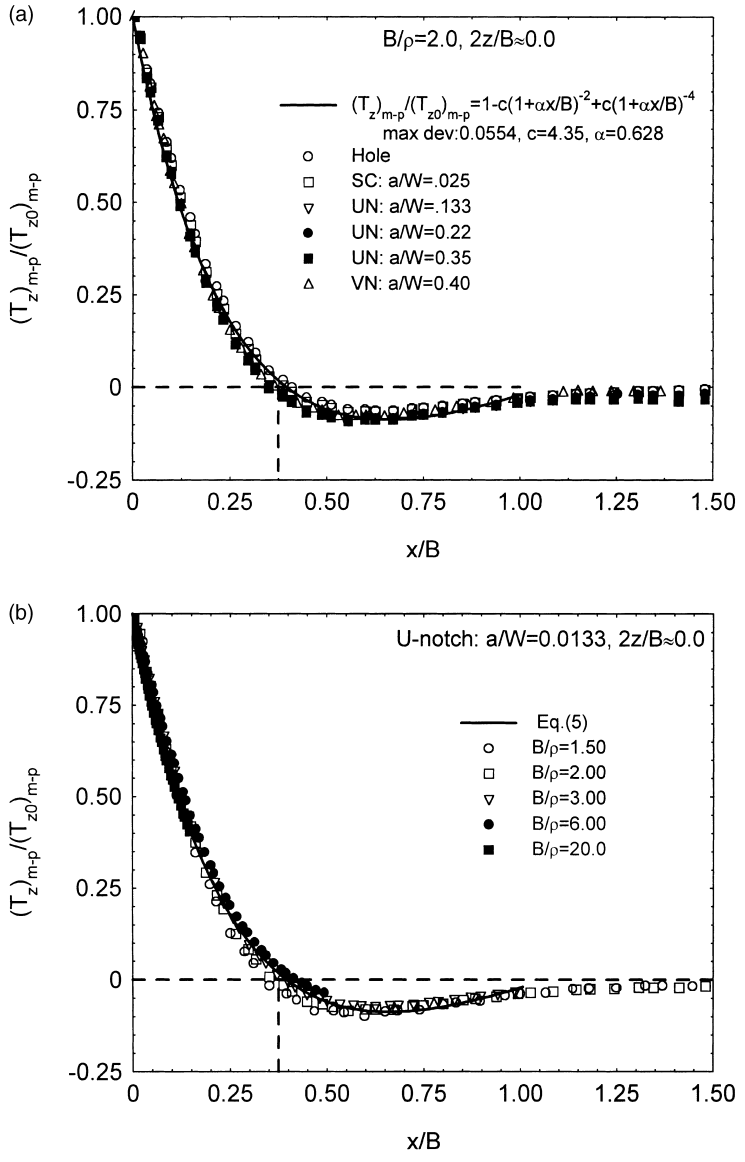

Fig. 4. The distribution of the out-of-plane constraint T_z on the mid-plane ahead of the notch root for (a) different notch configurations and, (b) different dimensionless thicknesses.

solution (5), the result predicted by Eq. (5) is also shown in Fig. 4(b). Obviously, solution (5) is in good agreement with 3D FE results of U-notches in different thickness plates.

For U-notches in plates with different dimensionless thickness, Fig. 5 gives the through-thickness variation of the 3D-effect zone size x^* (at which $T_z = 0$). The size of the 3D-effect zone is largest near the mid-plane, with a value of $x^*/B \approx 0.375$, and decreases with increasing $2z/B$ to zero on the free surface.

The through-thickness variation of T_{z0}, the out-of-plane constraint at the notch root, is shown in Fig. 6. In Fig. 6(a), the through-thickness variations of T_{z0} are plotted for different notch configurations, and are normalized by its corresponding value $(T_{z0})_{m-p}$ on the mid-plane. It is found that $T_{z0}/(T_{z0})_{m-p}$ is insensitive

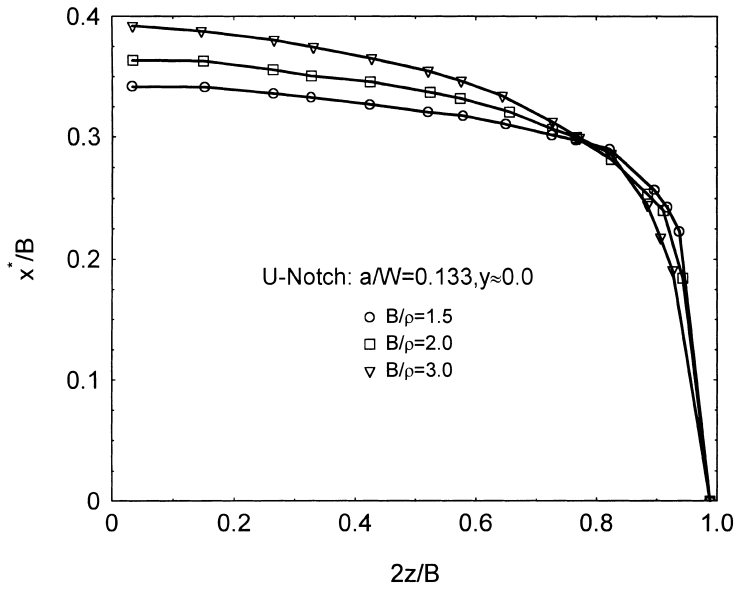

Fig. 5. The through-thickness variations of the size of 3D zone ($T_z \geqslant 0$) for different dimensionless thicknesses.

to the notch configuration. In Fig. 6(b), the through-thickness variations of T_{z0} are plotted for U-notches in plates of different thicknesses. The shape of the curve T_{z0}–$2z/B$ becomes flatter and flatter for decreasing B/ρ. But the normalized $T_{z0}/(T_{z0})_{m-p}$ is insensitive to a/W for different B/ρ as shown in Fig. 6(a). Consequently, $T_{z0}/(T_{z0})_{m-p}$ can be denoted as:

$$\frac{T_{z0}}{(T_{z0})_{m-p}} = g(B/\rho; 2z/B). \tag{6}$$

In Fig. 7, $(T_{z0})_{m-p}$ is plotted as a function of B/ρ. It is noted that in thin plates, $(T_{z0})_{m-p}$ increases with increasing B/ρ, while it approaches a saturated value when B/ρ is large enough. For the circular hole and semi-circular notch, the saturated value of $(T_{z0})_{m-p}$ is about 0.22 which is in good agreement with the theoretical result $2\nu/3$ by Sadowsky and Sternberg (1949) as $\nu = 0.333$ in this article. For U-notches with the depth $a/W = 0.133$ and $a/W = 0.22$, the saturated values of $(T_{z0})_{m-p}$ are 0.26 and 0.28, respectively. So, the plane strain state cannot be reached at the notch root with finite root radius no matter how thick the plate is. It can also be seen from Fig. 7 that the curves $(T_{z0})_{m-p} \sim B/\rho$ are essentially insensitive to the notch configuration when $B/\rho < 8$.

3.3. In-plane stress ratio

In Fig. 8, the in-plane stress ratio T_x in finite thickness plates is plotted against the distance x/ρ from notch root. Fig. 8(a) shows the distribution of the in-plane stress ratio $(T_x)_{m-p}$ on the mid-plane ahead of the notch-root for different notch depths and configurations. It is interesting to note that the distribution of $(T_x)_{m-p}$ at a small distance from the notch root ($x/\rho \leqslant 0.3$) is nearly the same for various notch configurations. Outside this region, $(T_x)_{m-p}$ becomes very sensitive to notch configurations. In Fig. 8(b) and (c), the changes of $(T_x)_{m-p}$ with the ratio B/ρ and T_x with $2z/B$ are given for U-notches. From Fig. 8(b), it can be seen that for a similar notch configuration, the distribution of $(T_x)_{m-p}$ ahead of the notch root is insensitive to B/ρ within $x/\rho \leqslant 0.5$. Fig. 8(c) shows that, in the vicinity of the notch root ($x/\rho \leqslant 0.5$), the distributions

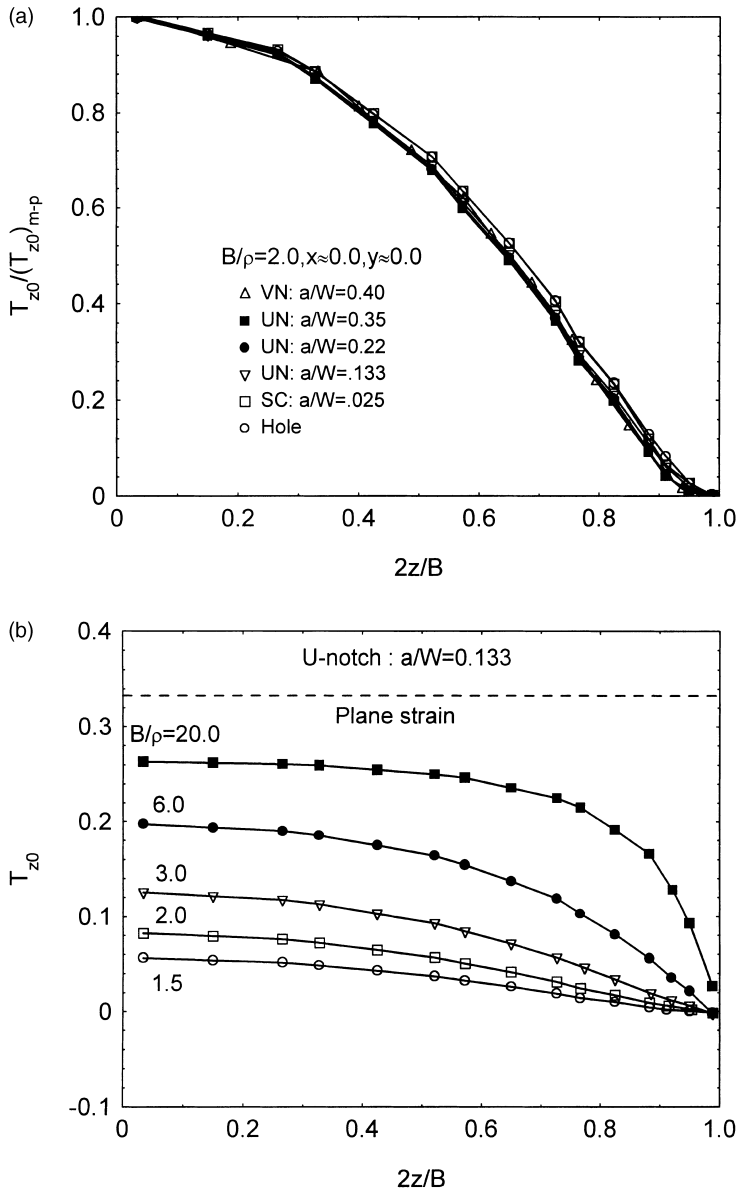

Fig. 6. The through-thickness variations of the out-of-plane constraint at notch root for (a) different notch configurations and, (b) different dimensionless thicknesses.

of T_x on different plane layers are very similar. Therefore, for different notch configurations and thicknesses, the in-plane stress ratio T_x near the notch root $(x/\rho \leqslant 0.3)$ can be uniformly expressed as:

$$T_x = h(x/\rho). \tag{7}$$

In 2D cases, when the SCF is introduced, the stress solution in an infinite plate having a circular hole can be obtained from the classical solution (Timoshenko and Goodier, 1970):

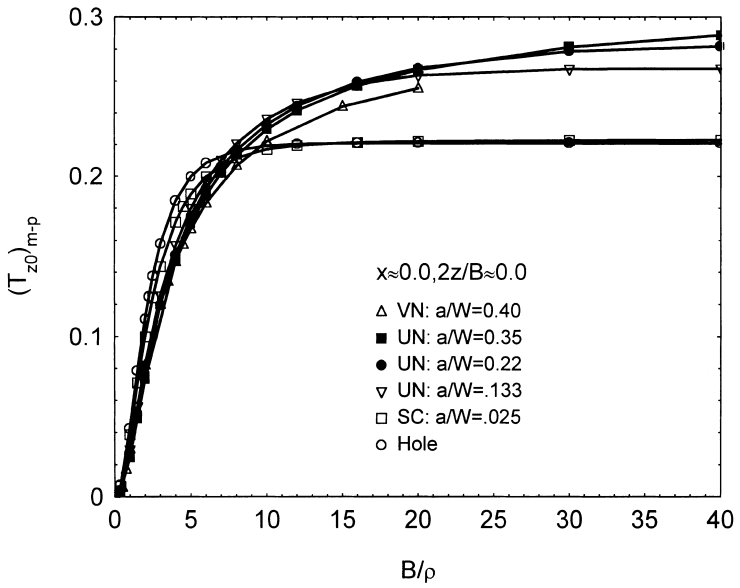

Fig. 7. The out-of-plane constraint on the mid-plane at notch root vs. the dimensionless thickness.

$$\begin{cases} \sigma_{xx} = \frac{K_t\sigma_y}{2}\left[\left(1+\frac{x}{\rho}\right)^{-2} - \left(1+\frac{x}{\rho}\right)^{-4}\right] \\ \sigma_{yy} = \frac{K_t\sigma_y}{3}\left[1+\frac{1}{2}\left(1+\frac{x}{\rho}\right)^{-2} + \frac{3}{2}\left(1+\frac{x}{\rho}\right)^{-4}\right] \end{cases} \tag{8}$$

It is easy to derive from Eq. (8) that

$$T_x = \frac{\left(1+\frac{x}{\rho}\right)^{-2} - \left(1+\frac{x}{\rho}\right)^{-4}}{\frac{2}{3}+\frac{1}{3}\left(1+\frac{x}{\rho}\right)^{-2} + \left(1+\frac{x}{\rho}\right)^{-4}}. \tag{9}$$

As reported by Glinka and Newport (1987), Creager and Paris's solution for blunt cracks can be used to estimate stress distribution near the tip of relatively deep notches:

$$\begin{cases} \sigma_{xx} = \frac{K_t\sigma_y}{2\sqrt{2}}\left[\left(\frac{1}{2}+\frac{x}{\rho}\right)^{-1/2} - \frac{1}{2}\left(\frac{1}{2}+\frac{x}{\rho}\right)^{-3/2}\right], \\ \sigma_{yy} = \frac{K_t\sigma_y}{2\sqrt{2}}\left[\left(\frac{1}{2}+\frac{x}{\rho}\right)^{-1/2} + \frac{1}{2}\left(\frac{1}{2}+\frac{x}{\rho}\right)^{-3/2}\right]. \end{cases} \tag{10}$$

It is easy to derive from Eq. (10) that

$$T_x = \frac{\left(\frac{1}{2}+\frac{x}{\rho}\right)^{-1/2} - \frac{1}{2}\left(\frac{1}{2}+\frac{x}{\rho}\right)^{-3/2}}{\left(\frac{1}{2}+\frac{x}{\rho}\right)^{-1/2} + \frac{1}{2}\left(\frac{1}{2}+\frac{x}{\rho}\right)^{-3/2}}. \tag{11}$$

Comparisons of solutions (9) and (11) with 3D FE results are given in Fig. 8(a). It can be seen that the 3D FE results of notches lie between 2D solutions (9) and (11). For a deeper 3D U-notch, solution (11) provides a good estimate of the in-plane stress ratio ahead of the notch root. For a circular hole, solution

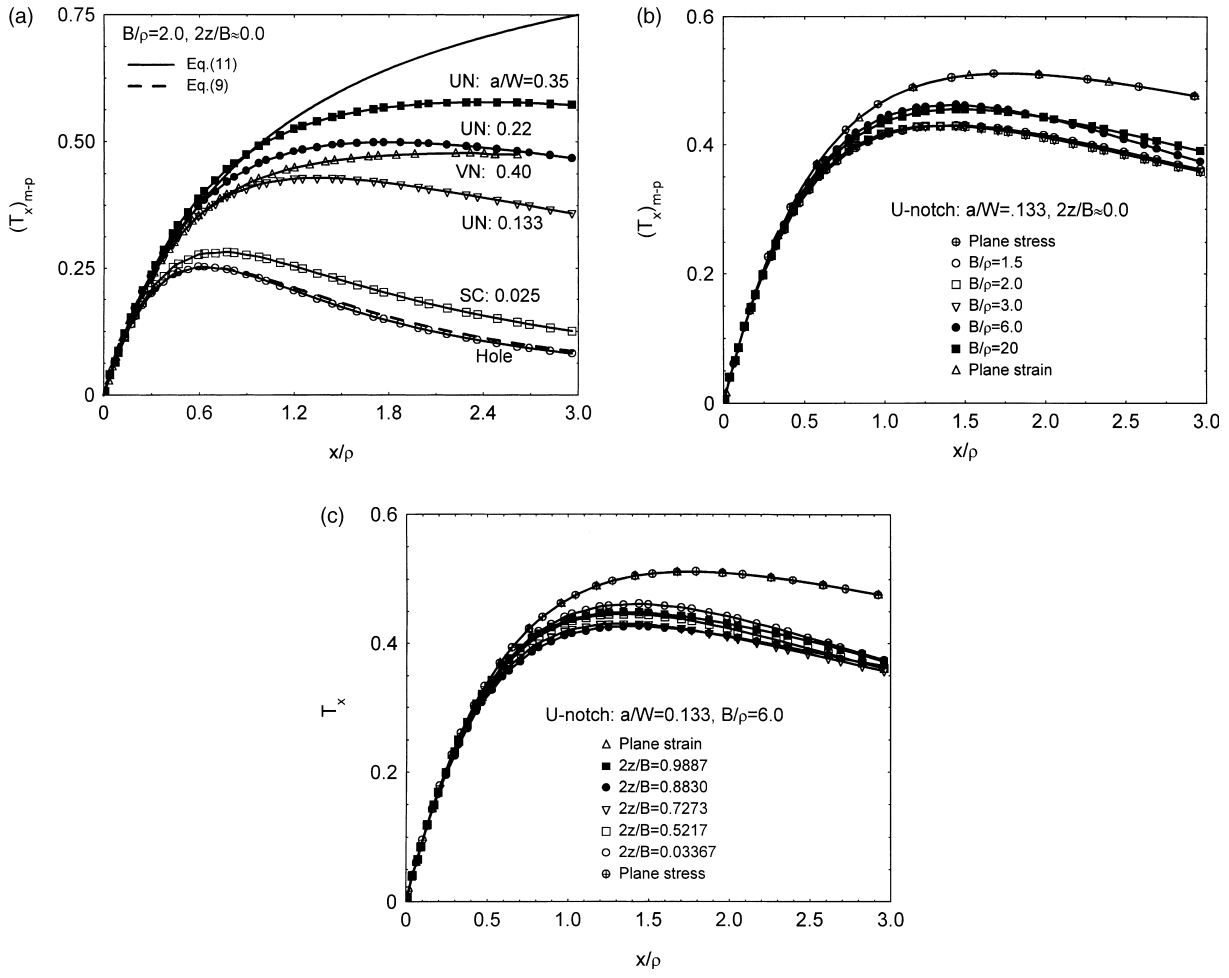

Fig. 8. The distribution of the in-plane stress ratio ahead of notch root on the mid-plane (a) for different notch configurations and, (b) for different dimensionless thicknesses and, (c) on different plane layers for $B/\rho = 6$.

(9) is nearly the same as the 3D solution of $(T_x)_{m-p}$. Obviously, the in-plane stress ratio near 3D notches $(x/\rho \leqslant 0.3)$ with arbitrary configurations can be predicted very well by the 2D solutions (9) or (11).

3.4. Near the notch front field

Fig. 9(a) and (b) shows the distribution of the opening stress $(\sigma_{yy})_{m-p}$ on the mid-plane for different notch configurations and dimensionless thicknesses. In this figure, the stress is normalized by the opening stress $(\sigma_{yy0})_{m-p}$ at the notch root, which is related to the SCF $(K_t)_{m-p}$ by $(\sigma_{yy0})_{m-p} = (K_t)_{m-p}\sigma_{\text{net}}$. It can be easily seen that the curves $(\sigma_{yy})_{m-p}/(\sigma_{yy0})_{m-p} \sim x/\rho$ are insensitive to the notch configuration within the 3D region $(0 \leqslant x/B \leqslant 0.375)$ (see Fig. 9(a)) and are completely independent of B/ρ (see Fig. 9(b)). On the mid-plane, 2D and 3D solutions of $(\sigma_{yy})_{m-p}/(\sigma_{yy0})_{m-p}$ coincide very well. Fig. 9(c) shows that the through-thickness variations of σ_{yy}/σ_{yy0}–x/ρ are very weak except in a very narrow region near the free surface $(2z/B > 0.9)$.

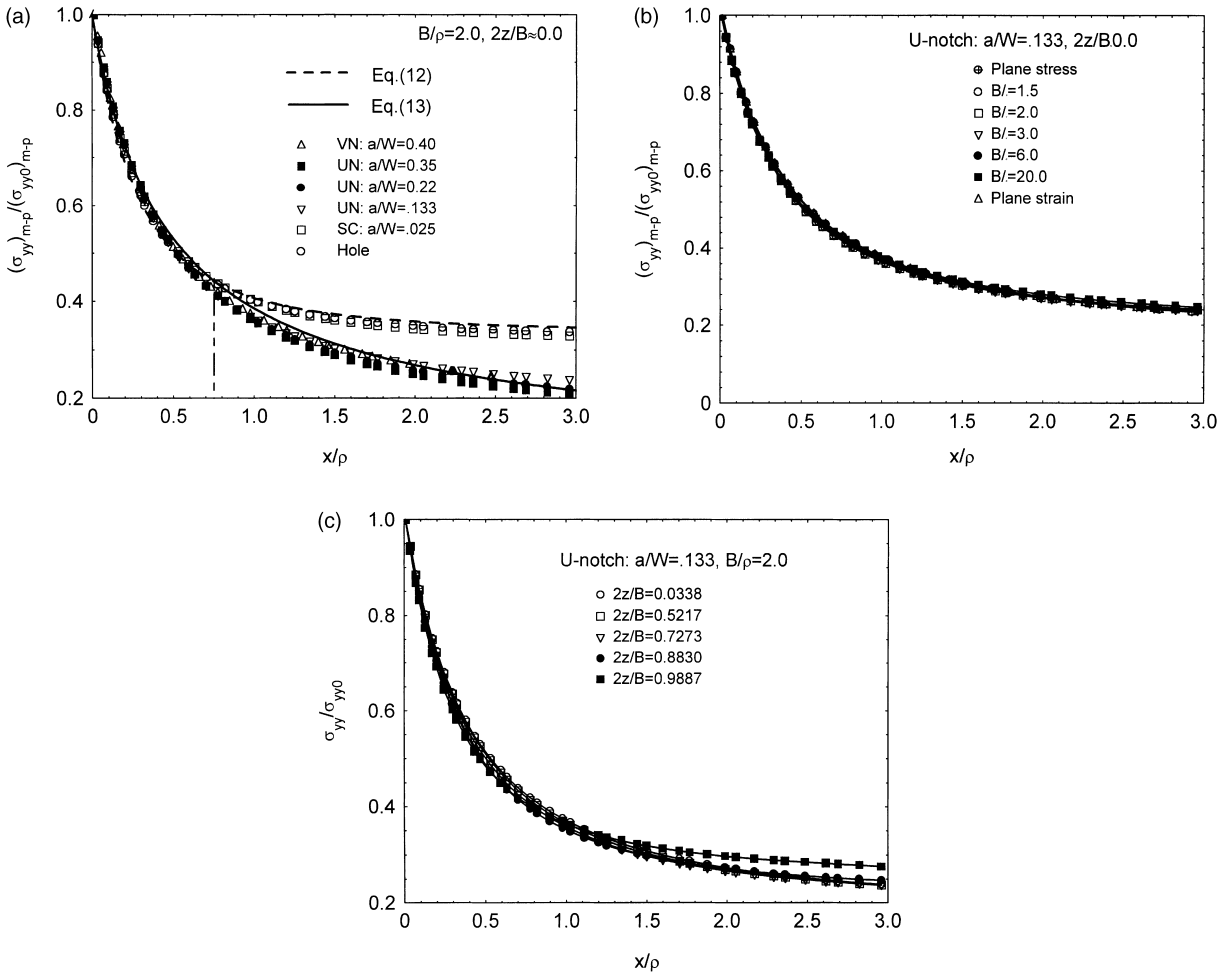

Fig. 9. The distribution of the opening stress ahead of notch-root on the mid-plane (a) for different notch configurations and, (b) for different dimensionless thicknesses and, (c) on different plane layers for $B/\rho = 2$.

In summary, the effect of thickness on the distribution of σ_{yy}/σ_{yy0} in front of the notch is very weak when the distance x from the notch root is normalized by ρ. So, it is reasonable to describe σ_{yy}/σ_{yy0} by the use of the 2D solution (8)

$$\frac{\sigma_{yy}}{\sigma_{yy0}} = \frac{1}{3}\left\{1 + \frac{1}{2}\left(1 + \frac{x}{\rho}\right)^{-2} + \frac{3}{2}\left(1 + \frac{x}{\rho}\right)^{-4}\right\} \tag{12}$$

or the Creager and Paris' 2D solution (10)

$$\frac{\sigma_{yy}}{\sigma_{yy0}} = \frac{1}{2\sqrt{2}}\left[\left(\frac{1}{2} + \frac{x}{\rho}\right)^{-\frac{1}{2}} + \frac{1}{2}\left(\frac{1}{2} + \frac{x}{\rho}\right)^{-\frac{3}{2}}\right]. \tag{13}$$

Comparisons of the 2D solutions (12) and (13) with 3D FE results are given in Fig. 9(a). For deeper U-notches, the normalized opening stress $(\sigma_{yy})_{m-p}/(\sigma_{yy0})_{m-p}$ on the mid-plane ahead of the 3D notch ($x/\rho < 3.0$) can be predicted well by the 2D solution (13). For a circular hole, the $(\sigma_{yy})_{m-p}/(\sigma_{yy0})_{m-p}$ in the

vicinity of the circular hole ($x/\rho < 3.0$) can be predicted well by the 2D solution (12). Obviously, for the 3D notches with different configurations, the normalized opening stress $(\sigma_{yy})_{m-p}/(\sigma_{yy0})_{m-p}$ near the 3D notches ($x/\rho < 0.75$) can be predicted very well by the 2D solutions (12) and (13) (see Fig. 9(a)).

The through-thickness variation of the out-of-plane strain component ε_{zz} is very important in simplifying the 3D finite thickness plate with free surfaces into a quasi-2D plate problem. Kane and Mindlin (1956) proposed a plate theory to take into account the thickness effect by assuming constant ε_{zz} through the

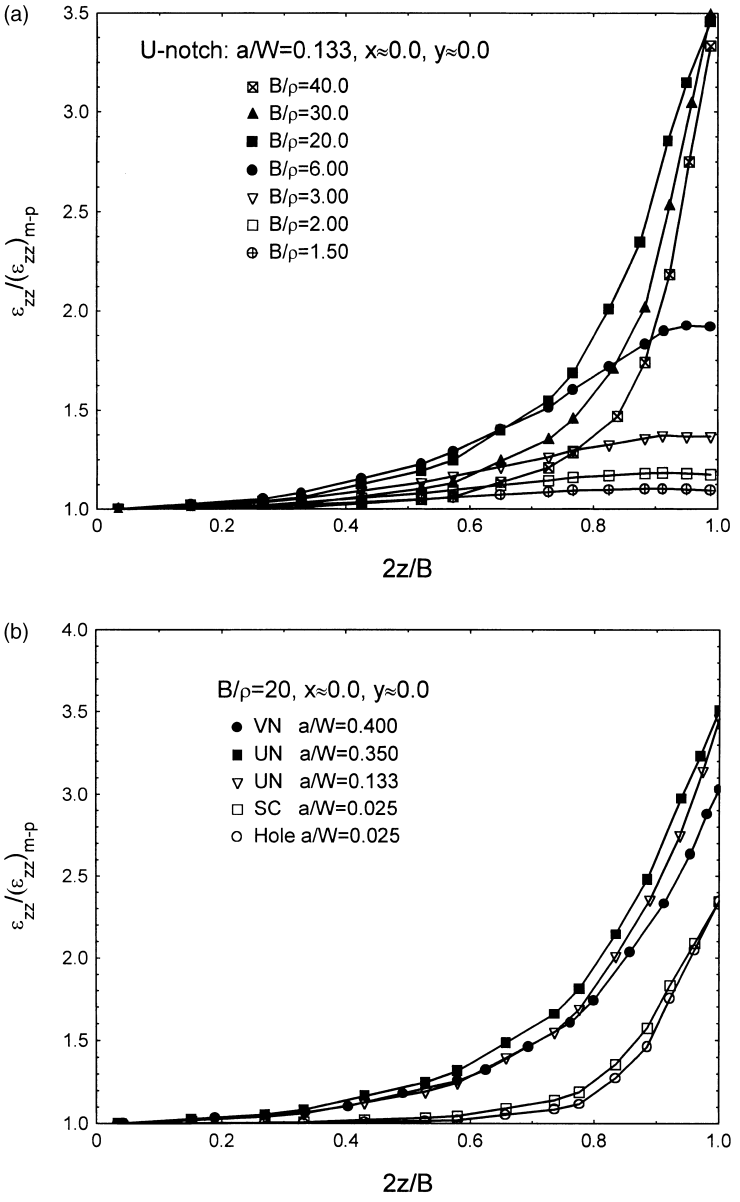

Fig. 10. The through-thickness variations of the out-of-plane strain ε_{zz} at the notch root for (a) different dimensionless thicknesses and, (b) different notch configurations.

thickness. This theory has been used for both the through-thickness crack (Yang and Freund, 1985) and the through-thickness circular hole (Krishnaswamy et al., 1998). However, the validations of this assumption in general notch problems cannot be found in the literature.

For double-edge U-notches in plates with different thicknesses, Fig. 10(a) shows the through-thickness variations of the out-of-plane strain ε_{zz} normalized by its corresponding value $(\varepsilon_{zz})_{m-p}$ at the mid-plane. It can be seen that the gradient of the out-of-plane strain is larger for greater B/ρ at the notch root. In a thin plate, the through-thickness variation of $\varepsilon_{zz}/(\varepsilon_{zz})_{m-p}$ is rather weak, less than 10% for $B/\rho < 1.5$. Therefore, for deeper notches, Kane–Mindlin's plate theory and similar ones assuming constant ε_{zz} through the thickness can be applied only to notch problems with small B/ρ. When B/ρ is greater than about 20, the region in the interior of the plate, where the variation of ε_{zz} is weak becomes larger as B/ρ increases. Therefore, the Kane–Mindlin assumption becomes better for a very thick plate except in a narrow layer near the free surface. We can draw an inference from the above analyses that for a sharp crack in a finite thickness plate, $B/\rho \to \infty$, $a/\rho \to \infty$, the Kane–Mindlin assumption will be fair in the interior of the plate, but it may not be reasonable to use this kind of assumption on the free surface.

Through-thickness variations of the distribution of ε_{zz} near the notch front with a notch depth a/W are presented in Fig. 10(b). In this figure, $B/\rho = 20$ is used, as around this value, the thickness effect on ε_{zz} is the most significant (see Fig. 10(a)). It is shown that when $a/W = 0.025$, the change of ε_{zz} is less than 10% within $2z/B < 0.8$. For a smaller a/W, $\varepsilon_{zz}/(\varepsilon_{zz})_{m-p}$ increases sharply as a/W increases, whereas when a/W becomes large (say greater than 0.133), the change of $\varepsilon_{zz}/(\varepsilon_{zz})_{m-p}$ with a/W is rather weak.

4. Conclusions

In the present article, extensive investigations of the elastic notch fields in finite thickness plates are made by recourse to the 3D FE method. Different notch configurations, notch depths and thicknesses to root-radius ratios are considered in this study. By comparison of 2D-notch fields and crack-tip fields, some special characters of the 3D-notch fields are revealed:

- SCFs at 3D-notch root have a close relation with the dimensionless plate thickness B/ρ and notch configurations. The SCFs in infinite thin or infinite thick plates will be the same as that in plane stress or plane strain states. For finite thickness plates, the SCFs at the notch root are greater than the corresponding 2D values. For circular holes or semi-circular notches, the SCF reaches its peak value which is about 5% higher than its 2D values at about $B/\rho = 3$. For deeper notches, the peak value is higher and occurs at a larger B/ρ. Before the peak value, the variation of the SCF with B/ρ is nearly independent of the notch configuration and depth.
- The variation of the opening stress normalized by $\sigma_{yy0} = K_t\sigma_y$ against the dimensionless distance x/ρ from the notch root is insensitive to the notch configuration and plate thickness, and can be predicted well by the use of the 2D solution for a circular hole or a blunt crack within $x/\rho \leqslant 0.75$.
- Due to the local stress concentration, the stress–strain fields have strong 3D effects in the neighborhood of the notch root. At least for notches with an opening angle less than 90°, the size of the 3D-effect zone ($T_z > 0$) is insensitive to notch geometry parameters and is about three-eighth plate thickness on the mid-plane. However, unlike the crack problems, due to the finite root radius, the stress state within the 3D zone cannot reach the plane strain state no matter how thick the plate is.
- On mid-plane, the variations of the normalized out-of-plane stress constraint factor $(T_z)_{m-p}/(T_{z0})_{m-p}$ against the dimensionless distance x/B are insensitive to plate thickness and notch configuration, and can be predicted well by Eq. (5), where $(T_{z0})_{m-p}$ is the value of $(T_z)_{m-p}$ at the notch root.
- Within a distance $x/\rho < 0.3$ from the notch root, the distribution of the in-plane stress ratio $T_x = \sigma_{xx}/\sigma_{yy}$ is insensitive to the plate thickness and the notch configuration, and can be described by the solution for a planar circular hole or blunt crack.

- In thin plates, the through-thickness variation of the out-of-plane strain ε_{zz} is weak and the Kane–Mindlin assumption can be used. But as dimensionless thickness B/ρ increases, the gradient of ε_{zz} increases steeply near the free surface. So, this kind of assumption is not suitable near the free surface. When the depth of the notch decreases, the errors of the Kane–Mindlin assumption become smaller.

Acknowledgements

The National Distinguished Young Scientist Fund and the National Natural Science Foundation of China supported this work. The authors wish to express their gratitude to Dr. T. Chang for helpful discussions.

References

Creager, M., Paris, P.C., 1967. Elastic field equations for blunt cracks with reference to stress corrosion cracking. Int. J. Fracture 3, 247–252.

Glinka, G., Newport, A., 1987. Universal features of elastic notch-tip stress fields. Int. J. Fatigue 9, 143–150.

Kane, T.R., Mindlin, R.D., 1956. High frequency extensional vibration of plates. J. Appl. Mech. 23, 277–283.

Krishnaswamy, S., Jin, Z.H., Batra, R.C., 1998. Stress concentration in an elastic Cosserat plate undergoing extensional deformations. J. Appl. Mech. 65, 66–70.

Kuang, Z.-B., 1982. The stress field near the blunt crack and the fracture criterian. Engng. Fract. Mech. 16, 19–33.

Kujawski, D., 1991. Estimations of stress intensity factors for small cracks at notches. Fatig. Fract. Engng. Mater. Struct. 14, 953–965.

Muskhelishvili, N.I., 1963. Some Basic Problems of the Mathematical Theory of Elasticity. Noordhoff, Groningen.

Nakamura, T., Parks, D.M., 1988. Three-dimensional stress field near the crack front of a thin elastic plate. J. Appl. Mech. 55, 805–813.

Nakamura, T., Parks, D.M., 1990. Three-dimensional crack front fields in a thin ductile plate. J. Mech. Phys. Solids 38, 787–812.

Savin, G.N., 1961. Stress Concentration around Holes. Pergamon Press, New York.

Shin, C.S., Man, K.C., Wang, C.M., 1994. A practical method to estimate the stress concentration of notches. Int. J. Fatigue 16, 242–256.

Sadowsky, M.A., Sternberg, E., 1947. Stress concentration around an ellipsoidal cavity in an infinite body under arbitrary plane stress perpendicular to the axis of revolution of the cavity. J. Appl. Mech. 14, A191–210.

Sadowsky, M.A., Sternberg, E., 1949. Stress concentration around a triaxial ellipsoidal cavity. J. Appl. Mech. 16, 149–157.

Sternberg, E., Sadowsky, M.A., Chicago, I.L.L., 1949. Three-dimensional solution for the stress concentration around a circular hole in a plate of arbitrary thickness. J. Appl. Mech. 16, 27–36.

Timoshenko, S., Goodier, J.N., 1970. Theory of Elasticity. McGraw Hill, New York, USA.

Xu, R.X., Thompson, J.C., Topper, T.H., 1996. Approximate expressions for three-dimensional notch tip stress fields. Fatig. Fract. Engng. Mater. Struct. 19, 893–902.

Xu, R.X., Thompson, J.C., Topper, T.H., 1995. Practical stress expressions for stress concentration regions. Fatig. Fract. Engng. Mater. Struct. 18, 885–895.

Yang, W., Freund, L.B., 1985. Transverse shear effects for through-cracks in an elastic plate. Int. J. Solids Struct. 21, 977–994.